Journal of Electroanalytical Chemistry 828 (2018) 137–143

Contents lists available at ScienceDirect

Journal of Electroanalytical Chemistry

journal homepage: www.elsevier.com/locate/jelechem

The aqueous deposition of a pH sensitive quinone on carbon paste electrodes using linear sweep voltammetry

Karen M. Herdman, Carmel B. Breslin, Niall J. Finnerty*

Chemistry Department, Maynooth University, Co. Kildare, Ireland

ARTICLE INFO

Keywords:
Continuous pH monitoring
Linear sweep voltammetry
Carbon paste electrodes
Nernstian response
Shelf-life

ABSTRACT

Herein, we report the electrodeposition of a quinone containing diazonium salt onto the surface of carbon paste electrodes (CPE). An extensive characterisation revealed the optimum deposition characteristics to be obtained using Linear Sweep Voltammetry (LSV) over the potential range +400 mV to −800 mV *vs.* SCE at 100 mV/s, for five sweeps in 0.1 M H_2SO_4. The corresponding FBRR-modified CPE was cycled in phosphate buffered saline over the potential range +800 mV to −700 mV *vs.* SCE at 100 mV/s. The anodic peak potential demonstrated excellent stability over 400 cycles and a Nernstian response was recorded (−59 ± 3 mV/pH, $n = 39$, $r^2 = 0.99$). The continuous monitoring of pH changes within the same solution exhibited Nernstian behaviour also, confirming the efficacy of the FBRR-modified CPEs for *in situ* pH monitoring. An extensive shelf-life investigation identified retention of FBRR-modified CPEs sensitivity over 28 days when stored under air conditions at 4 °C. The work described within confirms the effectiveness of FBRR-modified CPEs to perform continuous pH monitoring over a small pH range of physiological relevance.

1. Introduction

pH is a measurable parameter that is familiar to all in the scientific, industrial and medical fields [1]. The most commonly used pH sensor is the potentiometric glass electrode. The principal limitations associated with these electrodes are their large size and fragile nature, restricting their applications to *in vitro* bench top testing. For this reason, attempts to design robust, miniaturised, disposable and inexpensive pH electrodes have received much attention over the years. Metal oxide sensors utilise potentiometric measurements, are mechanically robust [2] and can easily be miniaturised using modern technologies. A wide range of metal oxide sensors have been reported including RuO_2 [3], PbO_2 [2,4] and IrOx [2,5]. The latter has demonstrated most promise due to a stable, quick response and broad pH recording range. Notwithstanding this, they still suffer from substantial drift over time and are susceptible to electrical noise interference [6]. Ion selective field effect transistors were introduced in 1970 [7]. They can be miniaturised readily [8], however, they suffer from a number of disadvantages including substantial drift [9], slow response [10,11], hysteresis effect, temperature dependence [12], high expense [1] and difficulties with encapsulation [13]. As an alternative to potentiometric pH electrodes, optical sensors have received close attention over the years. They have several advantages over potentiometric glass electrodes, including the ability to be miniaturised and lack of electrical interference [14]. However, they require large sized analytical equipment restricting their use to static investigations [15]. Other limitations include restricted long term stability, ionic strength affects [15], and a narrow working pH range, usually *ca.* 2–3 pH units [16].

Voltammetric pH sensors, which measure the redox potential of a pH dependent moiety, have demonstrated excellent performance in the past [17–19], are cost effective and easily miniaturised. The respective redox processes can be quantified using the Nernst equation, yielding the following response at 25 °C:

$$E = E^0 + (RT/F) \ln [a_{H}{}^{+}] \quad (1)$$

$$E = E^0 - (2.303RT/nF)\, pH \quad (2)$$

where E is the measured potential, E^0 is the standard electrode potential, R is the universal gas constant, T is the temperature in Kelvin, F is the Faraday constant and n is the number of electrons transferred. Potential is directly proportional to pH and reworking of the Nernst equation demonstrates that the observed potential for a redox system with m H^+ ions and n electrons transferred, will change by $-m/n$ (59 mV) per pH unit.

Carbon based materials and sensors have been widely used in the field of electrochemistry, because of their good electrical conductivity, ease of modification, low expense [4] and relatively wide operating

* Corresponding author at: Chemistry Department, Maynooth University, Ireland.
E-mail address: niall.finnerty@mu.ie (N.J. Finnerty).

https://doi.org/10.1016/j.jelechem.2018.09.049
Received 14 August 2018; Received in revised form 25 September 2018; Accepted 25 September 2018
Available online 26 September 2018

potential range [6]. Carbon materials can be functionalised by covalently attaching pH sensitive moieties, either by chemical or electrochemical processes; chemical or physical adsorption onto the surface; deposition of oxygen containing groups onto the electrode, or incorporation of the pH responsive substance into a composite electrode [20]. Many different carbon surfaces have been electrochemically modified with pH sensing elements, in particular, glassy carbon [21], carbon fibres (CFE) [22,23] and to a lesser extent carbon paste electrodes (CPE). The latter are inexpensive and easily modified, giving them pre-determined properties that makes them useful as highly selective sensors [24,25].

The first reported reduction of an aryl diazonium salt onto carbon was by Saveant and colleagues in 1992 [26]. More recently, Makos et al. described the electrodeposition of the quinone containing aryl diazonium salt, 4-Benzoylamino-2, 5-dimethoxybenzenediazonium chloride-hemi zinc chloride (FBRR) in aprotic solvent on CFEs using cyclic voltammetry [23]. However, the inherent fragility of the thin fibre, typically < 10 µm, and short term stability under physiological conditions [27], limits the adoption of CFEs into a broader range of applications. For these reasons they are most commonly utilised in acute monitoring of neurotransmitters in the brain extracellular fluid of rodents. CPEs are considerably larger, *ca.* 250 µm, more mechanically robust and demonstrate excellent long-term stability *in vivo* [28,29]. Therefore, the work described within details the electrodeposition of FBRR on CPEs. We postulated that impaired deposition of the diazonium salt will occur in an organic solvent since it is miscible with the hydrophobic layer on the surface of CPEs. This may result in the composite becoming dissolved, altering the surface morphology and impeding the electrochemical process [30]. Therefore, we proposed a more efficient deposition will proceed in aqueous media. Furthermore, we investigated the ability of linear sweep voltammetry (LSV) to deposit a more stable and uniform layer of the diazonium salt through application of the reduction sweep in isolation. Subsequently, the pH dependence of the deposited quinone was determined over a physiologically relevant pH range and shelf-life characteristics were elucidated.

2. Experimental

2.1. Chemicals and reagents

All reagents used *i.e.*, sodium chloride (NaCl), sodium hydroxide (NaOH), sodium hydrogen phosphate (NaH_2PO4), 4-Benzoylamino-2, 5-dimethoxybenzenediazonium chloride - hemi zinc chloride (FBRR), Acetonitrile (ACN), Tetraethyl Ammonium Tetrafluoroborate ($TEAFB_4$), Graphite Powder (< 20 µm, 1.9 g/cm^3) and Silicon Oil (0.96 g/mL) were purchased from Sigma Aldrich Chemical Co. (Dublin, Ireland). Sulfuric Acid was purchased from VWR International Ltd. (Dublin, Ireland). All calibrations were performed in phosphate buffered saline (PBS); NaCl (0.15 M), NaOH (0.04 M) and NaH_2PO4 (0.04 M) made up in doubly distilled deionised water. The pH was adjusted to 7.2, 7.4 and 7.6 using a laboratory pH meter (Eutech Instruments, Ayer Rajah, Singapore).

2.2. Electrode manufacture and deposition process

CPEs were manufactured from Teflon®-insulated silver (Ag) wire (200 µm bare diameter 8T, Advent Research Materials; Oxford, UK) using protocols previously described by others [31]. Briefly, a 5 cm length of Teflon insulated Ag wire was cut. Approximately 1 mm of the Teflon® insulation was removed from one end, exposing the bare Ag wire. Using a tweezers, the Teflon® was gently moved along the length of the wire, exposing a 1 mm cavity at the opposite end of the electrode. The exposed Ag wire was then soldered into a gold clip (Fine Science Tools GmbH, Heidelberg, Germany). The cavity was packed with carbon paste (0.71 g graphite powder and 250 µL silicon oil). A bare Ag wire with the same diameter, was used as a plunger, to ensure that the paste was compactly packed. The surface was levelled by gently rubbing it on a clean, flat surface. CPEs were modified with 2 mM FBRR in 0.1 M H_2SO_4 using LSV.

2.3. Cycling of FBRR-modified CPE in PBS

All calibrations were performed in a standard three-electrode glass electrochemical cell containing 20 mL PBS. The PBS was purged with nitrogen (N_2) gas (BOC Ireland) for 20 min to eliminate any interference from the reduction of oxygen that might be observed in the CV. Once cycling at one pH was complete, the electrodes were removed from one PBS solution, rinsed in deionised water and placed in another. The cycling order in the respective pH solutions was randomised between electrodes. A saturated calomel electrode (SCE) was used as the reference electrode and a large Pt wire served as the auxiliary electrode. FBRR-modified CPEs were cycled over the potential ranges −700 mV to +800 mV, −500 mV to +500 mV and −300 mV to +100 mV *vs.* SCE. Scan rates were varied between 20 and 1000 mV/s. The different experimental paradigms designed to determine the ability of the FBRR-modified CPEs to monitor pH changes continuously in solution are discussed in the relevant sections.

2.4. Instrumentation, software and data analysis

Voltammetric experiments were performed using a low-noise potentiostat (ACM Instruments, Cumbria, UK) and converted using an A/D converter (PowerLab, ADInstruments, Oxford, UK). The CV signals were recorded using eChem software (v2.1.16, eDAQ Ltd., Sydney, Australia) running on a Dell computer or laptop. All pH experiments were analysed using linear regressions. Significant differences were calculated using the Student's *t*-test for paired or unpaired observations, where appropriate. The standard 95% confidence interval was used for these tests, so a p-value < 0.05 indicated a significant difference between the two data sets, whereas a p-value higher than 0.05 indicated no significant difference. These analyses were performed using GraphPad Prism® version 5.01 (GraphPad Software Inc., San Diego, CA, USA). Scanning Electron Microscopy images (SEM) were carried out using a Hitachi S-3200-N to investigate CPE surface characteristics. Energy Dispersive X-Ray analysis (EDX) was performed using INCA x-act (Oxford Instruments) in conjunction with SEM to perform elemental analysis on the CPE.

3. Results and discussion

3.1. Optimisation of the electrodeposition of FBRR on CPEs

The electrochemical deposition of FBRR onto CPEs, in 0.1 M H_2SO_4, was achieved by a one-step electrochemical reduction process using LSV. The first step of the proposed mechanism involves the electrochemical reduction of the aryl diazonium cation (Ar-N_2^+) to form the corresponding aryl radical (Ar·), with the loss of N_2, as described in Eq. (3) [4,32]. This is a concerted reaction, therefore there are no intermediates formed between the cation and the radical formation, so the radical forms directly on the electrode surface [33]. The electrochemical reduction that leads to the formation of the radical is relatively easy because of the electron withdrawing power of the diazonium group [34]. The second step occurs when the radical reacts with the CPE surface, and a strong covalent C—C bond is formed according to Eq. (4).

$$ArN_2^+ + 1e^- \rightarrow Ar^{\cdot} + N_2 \quad (3)$$

$$Surface + Ar^{\cdot} \rightarrow Surface - Ar \quad (4)$$

Fig. 1A illustrates the LSV profiles for the electroreduction of FBRR onto CPEs. The anodic potential was varied from +200 mV to

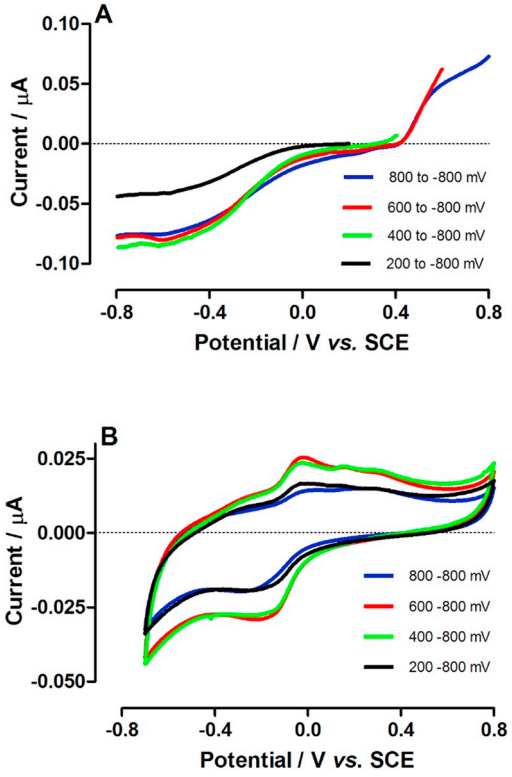

Fig. 1. (A) Average growth profiles of 4-Benzoylamino-2, 5-dimethoxybenzenediazonium chloride hemi zinc chloride (FBRR) in 0.1 M H_2SO_4 (n = 4) on carbon paste electrodes (CPEs) using Linear Sweep Voltammetry (LSV) (B) corresponding CVs of modified electrodes cycled in phosphate buffered saline (PBS, pH 7.4) over potential range – 700 mV to +800 mV *vs.* SCE at 100 mV/s (n = 4). Cycle 50 included for each CV.

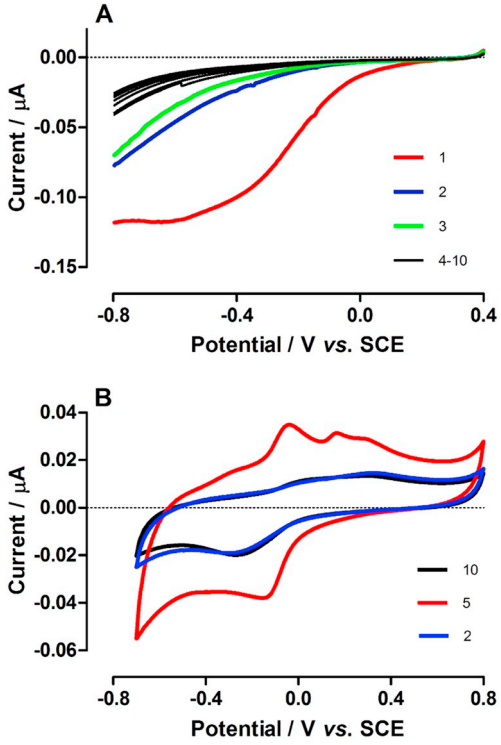

Fig. 2. (A) Average growth profiles of FBRR in 0.1 M H_2SO_4 onto CPEs using LSV over varying deposition sweeps (n = 4). (B) Average corresponding CVs of modified electrodes cycled in PBS (pH 7.4) over potential range – 700 mV to +800 mV *vs.* SCE at 100 mV/s (n = 4). Cycle 50 included for each CV.

+800 mV and the cathodic potential restricted to −800 mV *vs.* SCE at 100 mV/s. The limit of the reduction potential was chosen as −800 mV to avoid bringing the applied potential to too low a value resulting in the possible reduction of the aryl radical to the undesired anion [33,35], forming a multi-layered surface [36]. A reduction wave is evident which causes the radical formation of the FBRR and subsequent covalent bond formation with the CPE surface. It is apparent that the foot of the reductive wave occurs at a potential between −550 mV and −600 mV with maximum deposition occurring over the deposition ranges +400 mV and +600 mV to −800 mV *vs.* SCE. The corresponding CVs of the modified electrodes cycled in PBS (pH 7.4) are presented in Fig. 1B and follow a similar pattern with obvious redox peaks at −50 mV (anodic) and −150 mV (cathodic). The greater definition and resolution of the oxidation peaks are indicative of a more efficient electron transfer process. Conversely, the reduction peaks at *ca.* −150 mV appear much less resolved and more broad in definition suggesting slower electron transfer.

Subsequently, the effect of increasing deposition sweeps on the resolution of the FBRR redox peaks was investigated over the potential range +400 mV to −800 mV *vs.* SCE at 100 mV/s. The formation of a uniformly distributed monolayer of FBRR on the substrate is desirable in order to minimise the diffusion layer thickness therefore increasing the electron transfer kinetics. The electrochemical reduction of diazonium salts generally results in a layered deposition of the product onto the substrate, not monolayers [37]. These layers can vary in thickness from a few nm to several µm. The layers are formed when the radical attaches to the first layer of deposited FBRR. This happens when the radical attacks the *ortho*-position of an already surface bound aryl group, leading to the formation of multilayers. In principle, the application of more reduction sweeps should intuitively produce thicker layers [38]. Fig. 2A illustrates the average LSVs (n = 4) for 1–10 sweeps of FBRR deposition in H_2SO_4. It is apparent that most of the FBRR was deposited in the first sweep. The attachment of the aryl radical to the electrode surface gives rise to the near disappearance of the reduction curve. In the subsequent sweeps, the reduction peak is non-distinct which suggests that the electrode is in a passive state and FBRR is no longer depositing onto the CPE surface [33,35]. The corresponding CVs of the modified electrodes in PBS (pH 7.4) illustrate excellent peak definition (see Fig. 2B) with five sweeps producing maximum coverage. Conversely, 10 sweeps appeared to deposit too much FBRR on the surface, resulting in a multilayer deposition. This thick layer resulted in reduced electron transfer and therefore reduced peak currents. In addition, the peaks are also broader due to the slow rate of electron transfer. It is clearly evident from Fig. 2B that five sweeps of LSV deposition gives rise to optimum electrode coverage and clearly resolved oxidation peaks at *ca.* −20 mV and reduction peaks at *ca.* −150 mV when cycled in PBS. This gives a ΔE_p value of 130 mV *vs.* SCE. The redox pairs of quinones are generally classed as a quasi-reversible system, but this depends on the type of electrode used. At CPEs an irreversible behaviour is generally observed [39]. Our principal hypothesis, that optimum deposition would occur in aqueous solvent using LSV, is clearly illustrated in Fig. SM1. Peak definition was greatly compromised when deposition was performed in organic solvent and/or using cyclic voltammetry, lending strong support to our choice of analytical technique and solvent.

3.2. Optimisation of the FBRR-modified voltammogram

It was imperative to optimise the redox peak potentials of the FBRR-modified CPE and investigate the pH dependency of the deposited diazonium salt. In order to extrapolate these peak potentials, a sharp well-defined peak that is stable over time and responds to pH is desirable. Initially, we investigated the possibility of altering the potential window, to determine the effect on the respective peak resolution. Fig. SM2 illustrates the effect of varying the electrode potential range

(−700 mV to +800 mV, −500 mV to +500 mV and −300 to +100 mV *vs.* SCE) on peak definition. It is apparent that the larger window produced the most resolved peaks. The mechanism for the oxidation/reduction reaction of quinones, in buffered solutions, involves a $2e^-$ oxidation that converts the methoxy to the equivalent quinone, followed by a $2e^-/2H^+$ exchange to form the hydroxy-quinone [17,18,40]. The potentials at which the redox reactions take place are pH dependent, as the oxidation induces a loss of protons. The limit of the anodic and cathodic potentials were restricted to +800 and −700 mV respectively, to alleviate concerns about the possible interference of O_2 and H_2 evolution in the voltammogram. Furthermore, it is apparent that a sharper peak is consistently obtained for the anodic peak, lending support to its choice as the pH sensing site of the modified electrode. Greater variability in the cathodic peak definition, due to broader peaks, is indicative of a slower electron transfer process. This finding reduces its reliability in determining accurate peak potential shifts.

Next we investigated the effect of scan rate (ν) on the redox peaks by cycling the FBRR-modified CPEs from 20 to 1000 mV/s. In order to eliminate any hysteresis effects the electrodes were cycled from a slow scan rate of 20 mV/s increasing up to 1000 mV/s, the order was then reversed. By taking average peak currents of each scan rate, more accurate estimates of the currents were obtained. Fig. 3A plots the peak current (Ip) as a function of ν. R^2 values of 0.99 for the oxidation and reduction peak currents were achieved. Fig. 3B plots Ip as a function of the square root of the scan rate ($\nu^{1/2}$). R^2 values of 0.98 and 0.97 for the oxidation and reduction peak currents were achieved, respectively. As both these plots have straight line relationships a plot of the log of Ip *vs.* the log of the scan rate was constructed (see Fig. 3C). This gave a linear dependence with slopes of 0.82 and 0.92 for the oxidation and reduction peaks, respectively. These values, between 0.5 and 1.0, confirm mixed mass transport, diffusion and adsorption [41], resulting from thin layer diffusion [42,43]. This occurs when pockets of solution become trapped in the porous modified layer. As the electron transfer proceeds the currents decay over the potential cycle as there is a limited amount of FBRR in the trapped solution. These results are indicative of a quasi-reversible surface bound species that has been adsorbed onto the substrate surface [41]. Despite all peak currents increasing with ν, the oxidation peak at *ca.* +30 mV loses sharpness and definition at higher ν. Fig. 4A highlights the effect of increasing scan rates from 20 to

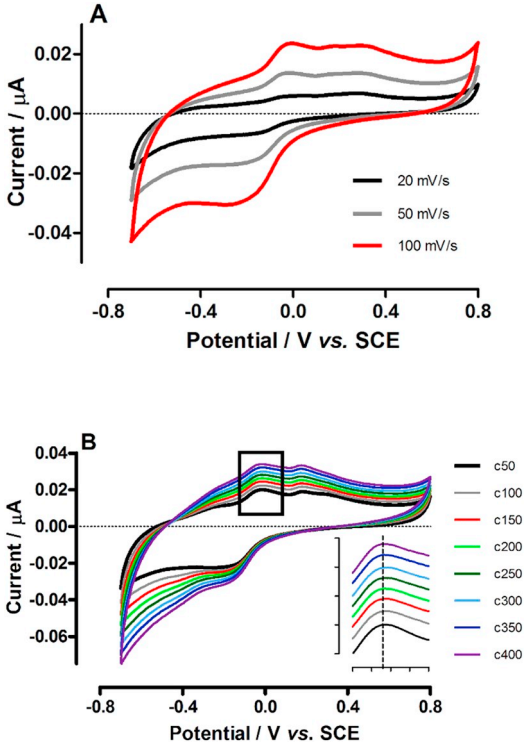

Fig. 4. Average CVs of FBRR-modified CPEs in PBS (pH 7.4) over potential range – 700 mV to +800 mV *vs.* SCE at 100 mV/s ($n = 4$). (A) Effect of scan rate on redox peak definition and (B) stability of anodic peak definition over 400 cycles. Inset: close up of anodic peaks.

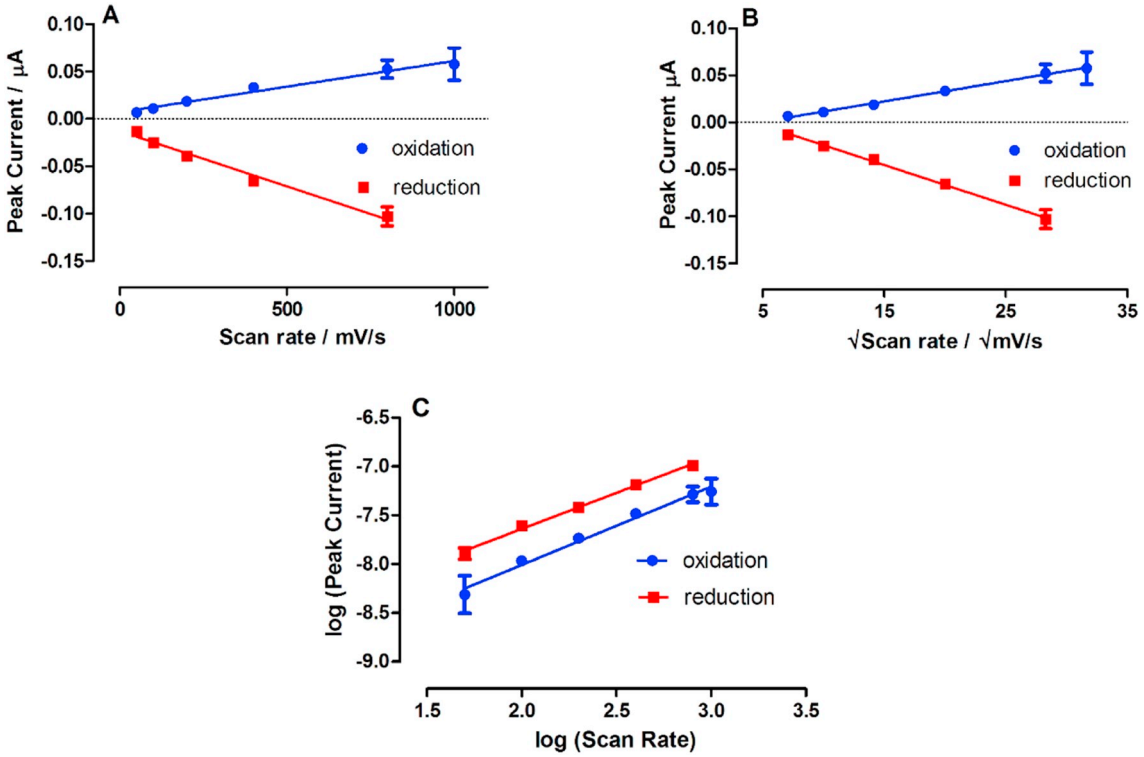

Fig. 3. XY plots of (A) peak current (Ip) *vs.* scan rate (ν), (B) Ip *vs.* $\nu^{1/2}$ and (C) log Ip *vs.* log ν, for FBRR-modified CPEs in PBS pH 7.4.

100 mV/s with optimum peaks recorded for 50 and 100 mV/s. The latter ν was chosen going forward to maximise sampling time.

A major limitation of existing pH sensors is their tendency to demonstrate drift over time, which results in them requiring frequent calibration [44]. To determine the stability of the oxidation peaks over time, the FBRR-modified CPEs were cycled in PBS for 400 cycles which equated to 200 min, at 100 mV/s. Fig. 4B details excellent stability of the oxidation peak potential over successive cycles (-28 ± 2 mV *vs.* SCE, $n = 32$). It is apparent that the peaks become more stable from cycle 100 onwards with minimum drift encountered. Furthermore, a concomitant increase in Ip is also recorded with continuous cycling. This gradual increase in Ip observed may be attributed to the binding oil leeching from the electrode [45] which culminates in increased conductivity [46] and increased surface area. Nevertheless, there is minimal compromise in peak resolution, lending support to the efficacy of the modified electrode at performing continuous monitoring. The presence of a second oxidation peak at *ca.* 350–400 mV is apparent in Figs. 2 and 3, which increases in magnitude at a slower rate than the quinone oxidation peak with cycling. It was postulated that this peak could be attributed to the $ZnCl_2$ present within the FBRR salt. To confirm its origin, a separate group of CPEs were subjected to electrodeposition in 0.5 to 2 mM $ZnCl_2$ over the same deposition potential, *i.e.* +400 mV to −800 mV at 100 mV/s. The corresponding CVs in PBS identified an oxidation peak at *ca.* 350–400 mV that increased in current with increasing $ZnCl_2$ concentrations (data not shown). Over the course of our investigations it became apparent that this peak associated with $ZnCl_2$ dissipated with subsequent depositions from the same FBRR solution. During the initial depositions, we hypothesised that the zinc was depositing onto the electrode surface more readily than the FBRR, therefore blocking available sites on the electrode surface. This produced concurrent oxidation peaks of similar magnitude which are clearly evident in Fig. 4B. This was further supported by Fig. SM3 which details SEM micrographs of a bare CPE and an FBRR modified CPE using LSV. The corresponding EDX image of the FBRR-modified CPE has peaks attributed to zinc deposition. Subsequent depositions produced voltammograms with reduced $ZnCl_2$ contribution and increasing FBRR anodic peak resolution. This was further confirmed by corresponding EDX images where no zinc peak was evident (data not shown). Therefore, all successive FBRR depositions incorporated an initial set of CPEs that were pre-reduced in FBRR to mitigate against this $ZnCl_2$ contribution. These electrodes were not utilised for any pH measurements and were disposed of. It is clearly obvious, from Fig. 5A, that the $ZnCl_2$ contribution has been negated using this step, lending strong support to our hypothesis.

3.3. pH dependence of redox peaks

As alluded to previously, the oxidation/reduction reaction of electrodeposited FBRR in buffered solutions, involves a $2e^-$ oxidation that converts the methoxy to the equivalent quinone, followed by a $2e^-/2H^+$ exchange to form the hydroxy-quinone. In accordance with the Nernst equation, cycling FBRR-modified CPEs in solutions of varying pH, should yield a slope value close to the ideal Nernstian response of −59 mV/pH. Fig. 5A details anodic peak separation for LSV deposited FBRR-modified CPEs, over three different pH ranges, for 100 cycles. The order of pH exposure was randomised in all investigations to mitigate against potential hysteresis effects. The vertical dashed line indicates the peak potential recorded for pH 7.4 (red trace) and is to be utilised as a point of reference for pH 7.2 (blue trace) and pH 7.6 (green trace). Fig. 5B illustrates the corresponding potential-pH profile for the oxidation peak. It is clearly evident that by varying pH, there is a reproducible shift in the FBRR oxidation peak potential. The peak potentials recorded in the respective pH solutions were as follows; pH 7.2: -14 ± 1 mV ($n = 39$), pH 7.4: -25 ± 1 mV ($n = 39$) and pH 7.6: -37 ± 1 mV ($n = 39$). The sensitivity value recorded for the process demonstrates Nernstian behaviour and excellent linearity over the chosen pH range (-59 ± 3 mV/pH, $n = 39$, $r^2 = 0.99$). This is a considerable improvement on a previously reported design, whereby linear regression analysis yielded a slope of 38 mV/pH unit on FBRR-modified CFEs, deposited in organic solvent [23]. A slight discrepancy was observed for the pH responses when recorded at cycle 50 (see Fig. SM4). The peak potentials recorded in the respective pH solutions were as follows; pH 7.2: -11 ± 2 mV ($n = 13$), pH 7.4: -24 ± 2 mV ($n = 13$) and pH 7.6: -40 ± 2 mV ($n = 13$). In this instance, the sensitivity value recorded for the process demonstrates a super-Nernstian response over the chosen pH range (-72 ± 5 mV/pH, $n = 13$, $r^2 = 0.99$). This finding supports our previous assumption that anodic peak stability is achieved from cycle 100 onwards. Super-Nernstian responses are not uncommon and the increased sensitivity may be a result of enhanced proton-exchange processes at the CPE surface or the number of H^+ ions amplified by transferred electrons [47].

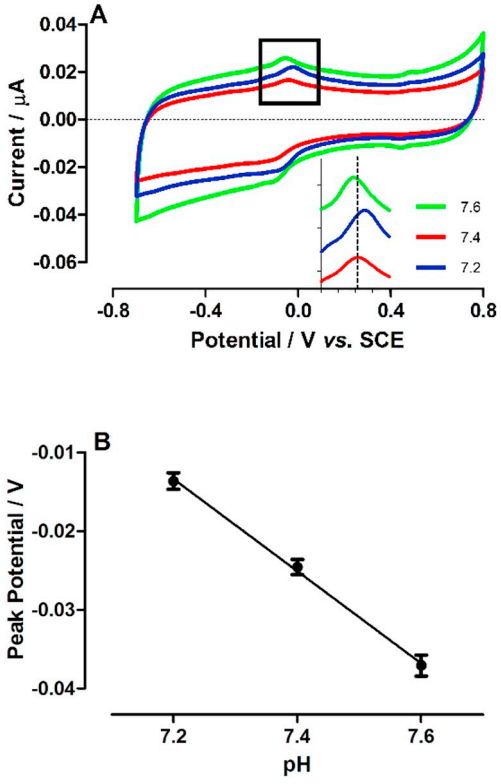

Fig. 5. (A) Effect of varying pH (7.2, 7.4 and 7.6) on oxidation peak potentials of FBRR-modified CPEs ($n = 4$) over −0.7 V to +0.8 V *vs.* SCE at 100 mV/s. Cycle 100 included for each pH. (B) Corresponding potential-pH profile and linear regression analysis (-59 ± 3 mV/pH) for oxidation peak potentials ($n = 39$). (For interpretation of the references to color in this figure, the reader is referred to the web version of this article.)

3.4. Continuous measurement of pH changes using FBRR-modified CPEs

The principal objective of these investigations was to determine the ability of the FBRR-modified CPEs to monitor pH changes within the same solution, mimicking more closely, eventual applications of the modified sensor. In this instance, the pH of the PBS solution was continuously monitored using a glass pH electrode in parallel to the FBRR-modified CPE being cycled between −700 mV to +800 mV *vs.* SCE. The peak potential was recorded every 20th and 50th cycle and correlated with the glass electrode pH. Aliquots of NaH_2PO_4 and NaOH were added to the PBS to shift the pH accordingly. The pH and anodic peak potential were correlated over successive cycling. As previous, the order of pH change was randomised in all investigations to mitigate against potential hysteresis effects. Fig. 6A highlights the effect of recording the pH and peak potential change every 20 and 50 cycles

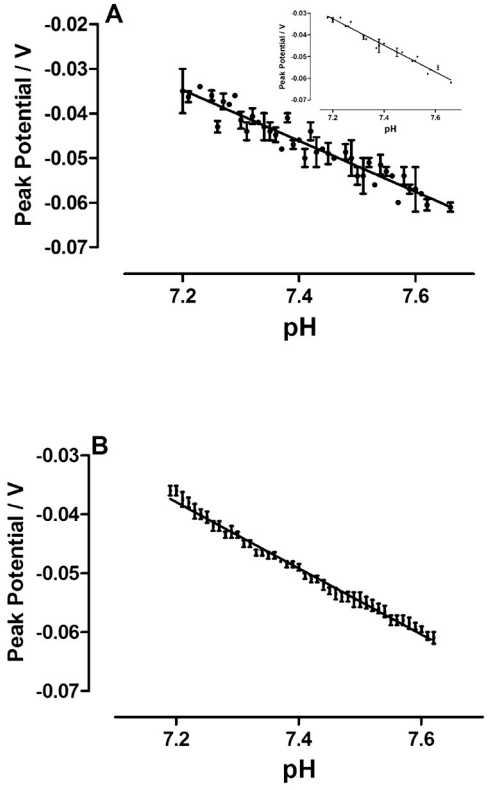

Fig. 6. (A) Continuous pH monitoring using FBRR-modified CPEs coupled with glass pH electrode, peak potential recorded every 20 cycles (n = 4). Inset: peak potential recorded every 50 cycles (n = 4). (B) Continuous pH monitoring using FBRR-modified CPEs coupled with Univentor syringe pump (n = 4).

respectively. The sensitivity values recorded demonstrate Nernstian behaviour and good linearity over the chosen pH range (-57 ± 2 mV/pH, n = 4, r^2 = 0.92 and -61 ± 3 mV/pH, n = 4, r^2 = 0.97).

One particular application for this FBRR-modified CPE could be to perform continuous monitoring of tissue pH under physiological conditions. In healthy individuals, tissue pH can vary between 7.35 and 7.45; anything outside 6.8 and 7.8 may result in irreversible cell damage and compromise in functionality. A sensor that can measure physiological relevant pH changes, *i.e.* with precision greater than or equal to 0.02 pH units, is therefore highly desirable. A similar experimental set-up to that described in Fig. 6A was implemented, however, a microinfusion pump was incorporated into the design to facilitate a more reproducible method of shifting the pH by approximately 0.01 units. The FBRR-modified CPEs were cycled for a minimum of 50 cycles prior to commencement of peak potential recordings. NaH_2PO_4 and NaOH were infused at a constant flow rate of 5 µL/min and the voltammogram was continuously cycled between −700 mV to +800 mV *vs.* SCE and the pH limits of 7.2 to 7.6. The PBS was constantly stirred at a rate of *ca.* 45 rev/min. The cycle number and time were recorded for each 0.01 pH unit shift and the peak potentials were extrapolated once the experiment was completed. Fig. 6B highlights the effectiveness of the sensor at measuring these minute pH changes and the sensitivity value recorded demonstrated close to Nernstian behaviour and good linearity over the chosen pH range (-56 ± 1 mV/pH, n = 4, r^2 = 0.95). The small error bars are equivalent to *ca.* 2 mV which corresponds to 0.03 pH units. These results demonstrate the efficacy of the FBRR-modified CPEs at measuring continuous changes in solution pH over long periods.

3.5. Shelf-life characteristics of FBRR-modified CPEs

The effect of storage on the longevity of FBRR-modified CPEs was investigated. Separate sets of electrodes (n = 4) were used in each instance to mitigate against the effect of repeated calibrations on electrode performance [48]. The longevity of a modified electrode is an important characteristic to elucidate since it facilitates the bulk manufacture of FBRR-modified CPEs prior to their application in specific investigations. Table 1 details the effect of storing the modified electrodes at 4 °C subsequent to calibration in the respective pH solutions. It is apparent that the sensitivity *i.e.* pH response, shifted more towards Nernstian behaviour following storage. This could be attributed to the carbon paste becoming homogenised [49]. Notwithstanding this, there was no significant difference observed between day 0 and day 1–28 of storage. The slight discrepancy in day 0 sensitivities can be attributed to the porous, surface irregularities associated with CPE. Conversely, the longevity of FBRR-modified CPEs was compromised when stored under N_2 conditions at 4 °C. Table SM1 identifies significant differences in sensitivities recorded between day 0 and day 1 and day 0 and day 7. Furthermore, a decrease in sensitivity was recorded across most days of storage. Collectively, these findings support the longevity of the FBRR-modified CPEs for 28 days when stored under air conditions at 4 °C.

Table 1
Summary of shelf-life characteristics of FBRR-modified CPE stored at 4 °C.

	Slope mV/pH	SEM	r^2	n	p-Value
Day 0	−63.8	2.2	0.99	4	0.64
+1 Day	−62.1	2.6	0.99	4	
Day 0	−61.7	4.4	0.99	4	0.60
+3 Days	−58.8	2.2	0.99	4	
Day 0	−62.0	3.5	0.99	4	0.76
+7 Days	−60.8	1.9	0.99	4	
Day 0	−61.3	2.2	0.99	4	0.65
+14 Days	−60.0	1.4	0.99	4	
Day 0	−56.3	0.7	0.99	4	0.79
+28 Days	−57.5	4.3	0.99	4	

4. Conclusion

We have described within, the electrodeposition of the quinone containing diazonium salt, FBBR, onto the surface of CPE. We investigated the effect of the deposition window and cycle number in 0.1 M H_2SO_4 using LSV. Optimum deposition occurred over the potential range +400 mV to −800 mV *vs.* SCE at 100 mV/s, for five sweeps. Excellent peak resolution was confirmed for the FBRR-modified CPEs when cycled in PBS of varying pH over the potential range +800 to −700 mV *vs.* SCE. The anodic peak potential was confirmed to be stable for up to 400 cycles and demonstrated Nernstian behaviour in PBS of varying pH. A method of performing continuous pH measurements from within the same solution confirmed the efficacy of the FBRR-modified CPEs for *in situ* pH monitoring, with Nernstian behaviour demonstrated once more. Finally, an extensive shelf-life investigation identified retention of FBRR-modified CPEs sensitivity over 28 days when stored under air conditions at 4 °C. The work described supports the feasibility of FBRR-modified CPEs to perform continuous pH monitoring across a physiologically relevant range. Furthermore, it strongly supports an extensive *in vitro* characterisation be undertaken to confirm its ability at performing physiological monitoring.

Acknowledgements

All work described within was undertaken through financial support from the Irish Research Council (Grant no. RS/2012/79). We also extend our gratitude to Prof. John Lowry for providing access to infrastructure.

Conflict of interest

The authors have no conflict of interest.

Appendix A. Supplementary data

Supplementary data to this article can be found online at https://doi.org/10.1016/j.jelechem.2018.09.049.

References

[1] W.-D. Huang, H. Cao, S. Deb, M. Chiao, J.C. Chiao, A flexible pH sensor based on the iridium oxide sensing film, Sensors Actuators A 169 (1) (2011) 1–11.
[2] X.-r. Huang, Q.-q. Ren, X.-j. Yuan, W. Wen, W. Chen, D.-p. Zhan, Iridium oxide based coaxial pH ultramicroelectrode, Electrochem. Commun. 40 (2014) 35–37.
[3] Y.-H. Liao, J.-C. Chou, Preparation and characteristics of ruthenium dioxide for pH array sensors with real-time measurement system, Sensors Actuators B 128 (2) (2008) 603–612.
[4] H. Kahlert, Functionalized carbon electrodes for pH determination, J. Solid State Electrochem. 12 (10) (2008) 1255–1266.
[5] M. Wang, S. Yao, M. Madou, A long-term stable iridium oxide pH electrode, Sensors Actuators B 81 (2–3) (2002) 313–315.
[6] P. Takmakov, M.K. Zachek, R.B. Keithley, E.S. Bucher, G.S. McCarty, R.M. Wightman, Characterization of local pH changes in brain using fast-scan cyclic voltammetry with carbon microelectrodes, Anal. Chem. 82 (2010) 9892–9900.
[7] P. Bergveld, Development of an ion-sensitive solid-state device for neurophysiological measurements, IEEE Trans. Biomed. Eng. 17 (1) (1970) 70–71.
[8] M.M. Maharbiz, W.J. Holtz, R.T. Howe, J.D. Keasling, Microbioreactor arrays with parametric control for high-throughput experimentation, Biotechnol. Bioeng. 85 (4) (2004) 376–381.
[9] C. Cane, I. Gracia, A. Merlos, Microtechnologies for pH ISFET chemical sensors, Microelectron. J. 28 (4) (1997) 389–405.
[10] P. Duroux, C. Emde, P. Bauerfeind, C. Francis, A. Grisel, L. Thybaud, D. Arstrong, C. Depeursinge, A.L. Blum, The ion sensitive field effect transistor (ISFET) pH electrode: a new sensor for long term ambulatory pH monitoring, Gut 32 (3) (1991) 240–245.
[11] J.A. Voorthuyzen, P. Bergveld, Photoelectric effects in tantalum pentoxide-silicon dioxide-silicon structures, Sensors Actuators B 1 (1–6) (1990) 350–353.
[12] P. Kurzweil, Metal oxides and ion-exchanging surfaces as pH sensors in liquids: state-of-the-art and outlook, Sensors 9 (6) (2009) 4955–4985.
[13] C. Demuth, J. Varonier, V. Jossen, R. Eibl, D. Eibl, Novel probes for pH and dissolved oxygen measurements in cultivations from millilitre to benchtop scale, Appl. Microbiol. Biotechnol. 100 (9) (2016) 3853–3863.
[14] J. Lin, Recent development and applications of optical and fiber-optic pH sensors, Trends Anal. Chem. 19 (9) (2000) 541–552.
[15] O. Korostynska, K. Arshak, E. Gill, A. Arshak, Review paper: materials and techniques for in vivo pH monitoring, IEEE Sensors J. 8 (1) (2008) 20–28.
[16] D. Wencel, T. Abel, C. McDonagh, Optical chemical pH sensors, Anal. Chem. 86 (1) (2014) 15–29.
[17] M. Lu, R.G. Compton, Voltammetric pH sensor based on an edge plane pyrolytic graphite electrode, Analyst 139 (10) (2014) 2397–2403.
[18] M. Lu, R.G. Compton, Voltammetric pH sensing using carbon electrodes: glassy carbon behaves similarly to EPPG, Analyst 139 (18) (2014) 4599–4605.
[19] M. Michalak, M. Kurel, J. Jedraszko, D. Toczydlowska, G. Wittstock, M. Opallo, W. Nogala, Voltammetric pH nanosensor, Anal. Chem. 87 (23) (2015) 11641–11645.
[20] H.C. Leventis, I. Streeter, G.G. Wildgoose, N.S. Lawrence, L. Jiang, T.G.J. Jones, R.G. Compton, Derivatized carbon powder electrodes: reagentless pH sensors, Talanta 63 (4) (2004) 1039–1051.
[21] K.K. Shiu, F. Song, H.P. Dai, Potentiometric pH sensor with anthraquinonesulfonate adsorbed on glassy carbon electrodes, Electroanalysis 8 (1996) 1160–1164.
[22] A. Anderson, J. Phair, J. Benson, B. Meenan, J. Davis, Investigating the use of endogenous quinoid moieties on carbon fibre as means of developing micro pH sensors, Mater. Sci. Eng. C 43 (2014) 533–537.
[23] M.A. Makos, D.M. Omiatek, A.G. Ewing, M.L. Heien, Development and characterization of a voltammetric carbon-fiber microelectrode pH sensor, Langmuir 26 (2010) 10386–10391.
[24] I. Svancara, K. Vytras, J. Barek, J. Zima, Carbon paste electrodes in modern electroanalysis, Crit. Rev. Anal. Chem. 31 (4) (2001) 311–345.
[25] K. Kalcher, I. Svancara, M. Buzuk, K. Vytras, A. Walcarius, Electrochemical sensors and biosensors based on heterogeneous carbon materials, Monatsh. Chem. 140 (2009) 861–889.
[26] M. Delamar, R. Hitmi, J. Pinson, J.M. Saveant, Covalent modification of carbon surfaces by grafting of functionalized aryl radicals produced from electrochemical reduction of diazonium salts, J. Am. Chem. Soc. 114 (1992) 5883–5884.
[27] D.A. Kane, R.D. O'Neill, Major differences in the behaviour of carbon paste and carbon fibre electrodes in a protein-lipid matrix: implications for voltammetry in vivo, Analyst 123 (1998) 2899–2903.
[28] R.N. Adams, Probing brain chemistry with electroanalytical techniques, Anal. Chem. 48 (14) (1976) 1126A–1138A.
[29] D.E. Ormonde, R.D. O'Neill, The oxidation of ascorbic acid at carbon paste electrodes. Modified response following contact with surfactant, lipid and brain tissue, J. Electroanal. Chem. Interfacial Electrochem. 279 (1990) 109–121.
[30] M.E. Rice, Z. Galus, R.N. Adams, Graphite paste electrodes. Effects of paste composition and surface states on electron-transfer rates, J. Electroanal. Chem. Interfacial Electrochem. 143 (1–2) (1983) 89–102.
[31] F.B. Bolger, R. Bennett, J.P. Lowry, An in vitro characterisation comparing carbon paste and Pt microelectrodes for real-time detection of brain tissue oxygen, Analyst 136 (19) (2011) 4028–4035.
[32] A.J. Downard, Electrochemically assisted covalent modification of carbon electrodes, Electroanalysis 12 (14) (2000) 1085–1096.
[33] J. Pinson, Attachment of organic layers to materials surfaces by reduction of diazonium salts, in: M. Chehimi (Ed.), Aryl Diazonium Salts: New Coupling Agents in Polymer and Surface Science, Wiley-VCH Verlag GmbH & Co. KGaA, 2012, pp. 1–35.
[34] J.J. Gooding, Advances in interfacial design for electrochemical biosensors and sensors: aryl diazonium salts for modifying carbon and metal electrodes, Electroanalysis 20 (2008) 573–582.
[35] J. Pinson, F. Podvorica, Attachment of organic layers to conductive or semiconductive surfaces by reduction of diazonium salts, Chem. Soc. Rev. 34 (2005) 429–439.
[36] J.K. Kariuki, M.T. McDermott, Formation of multilayers on glassy carbon electrodes via the reduction of diazonium salts, Langmuir 17 (19) (2001) 5947–5951.
[37] H. Salehzadeh, D. Nematollahi, V. Khakyzadeh, B. Mokhtari, L.C. Henderson, General approach for electrochemical functionalization of glassy carbon surface by in situ generation of diazonium ion under acidic and non-acidic condition with a cascade protocol, Electrochim. Acta 139 (2014) 270–280.
[38] M. Raicopol, L. Necula, M. Ionita, L. Pilan, Electrochemical reduction of aryl diazonium salts: a versatile way for carbon nanotubes functionalisation, Surf. Interface Anal. 44 (2012) 1081–1085.
[39] J. Lindquist, Seven different carbon paste electrodes, J. Electroanal. Chem. Interfacial Electrochem. 52 (1) (1974) 37–46.
[40] C.C.M. Neumann, C. Batchelor-McAuley, C. Downing, R.G. Compton, Anthraquinone monosulfonate adsorbed on graphite shows two very different rates of electron transfer: surface heterogeneity due to basal and edge plane sites, Chem. Eur. J. 17 (26) (2011) 7320–7326.
[41] M.J. Sims, N.V. Rees, E.J.F. Dickinson, R.G. Compton, Effects of thin-layer diffusion in the electrochemical detection of nicotine on basal plane pyrolytic graphite (BPPG) electrodes modified with layers of multi-walled carbon nanotubes (MWCNT-BPPG), Sensors Actuators B 144 (1) (2010) 153–158.
[42] I. Streeter, G.G. Wildgoose, L. Shao, R.G. Compton, Cyclic voltammetry on electrode surfaces covered with porous layers: an analysis of electron transfer kinetics at single-walled carbon nanotube modified electrodes, Sensors Actuators B 133 (2) (2008) 462–466.
[43] G. Yildiz, Z. Aydogmus, J.-M. Kauffmann, Differential pulse voltammetric determination of montelukast in tablets and human plasma by using chitosan modified carbon paste electrode, Electroanalysis 25 (2013) 1796–1802.
[44] G.G. Wildgoose, M. Pandurangappa, N.S. Lawrence, L. Jiang, T.G.J. Jones, R.G. Compton, Anthraquinone-derivatised carbon powder: reagentless voltammetric pH electrodes, Talanta 60 (5) (2003) 887–893.
[45] P.D. Lyne, R.D. O'Neill, Stearate-modified carbon paste electrodes for detecting dopamine in vivo: decrease in selectivity caused by lipids and other surface-active agents, Anal. Chem. 62 (1990) 2347–2351.
[46] K. Kalcher, J.M. Kauffmann, J. Wang, I. Svancara, K. Vytras, C. Neuhold, Z. Yang, Sensors based on carbon paste in electrochemical analysis: a review with particular emphasis on the period 1990–1993, Electroanalysis 7 (1) (1995) 5–22.
[47] N.J. Finnerty, F.B. Bolger, A platinum oxide-based microvoltammetric pH electrode suitable for physiological investigations, Analyst 143 (2018) 3124–3133.
[48] A.M. Wynne, N.J. Finnerty, Ascorbic acid rejection characteristics of modified platinum electrodes: a shelf life investigation, Chem. Aust. 3 (2) (2015) 55–69.
[49] I. Svancara, M. Hvizdalova, K. Vytras, K. Kalcher, R. Novotny, A microscopic study on carbon paste electrodes, Electroanalysis 8 (1996) 61–65.